

Nonequilibrium interactions between two quantum circuits

V.S. Khrapai^{1,2}, S. Ludwig¹, J.P. Kotthaus¹ and H.P. Tranitz³, W. Wegscheider³

¹ *Center for NanoScience and Department für Physik,*

Ludwig-Maximilians-Universität, Geschwister-Scholl-Platz 1, D-80539 München,

Germany; ² Institute of Solid State Physics RAS, Chernogolovka, 142432,

Russian Federation; ³ Institut für Experimentelle und Angewandte Physik,

Universität Regensburg, D-93040 Regensburg, Germany

Abstract

We briefly overview our recent results on nonequilibrium interactions between neighboring electrically isolated nanostructures. One of the nanostructures is represented by an externally biased quantum point contact (drive-QPC), which is used to supply energy quanta to the second nanostructure (detector). Absorption of these nonequilibrium quanta of energy generates a dc-current in the detector, or changes its differential conductance. We present results for a double quantum dot, a single quantum dot or a second QPC placed in the detector circuit. In all three cases a detection of quanta with energies up to ~ 1 meV is possible for bias voltages across the drive-QPC in the mV range. The results are qualitatively consistent with an energy transfer mechanism based on nonequilibrium acoustic phonons.

I. INTRODUCTION

Present GaAs fabrication techniques enable one to create a pair of nanostructures connected to separate two-dimensional electron gas (2DEG) leads and placed just about 100 nm apart. Out of thermodynamic equilibrium a net transfer of energy between such two circuits can occur owing to a direct Coulomb interaction, electron-photon and electron-phonon interactions. Which interaction is dominating the energy transfer in a particular case is not known *a priori*.

Regardless the type of interaction, the change of energy/momentum of an electron satisfies the conservation laws. The conservation of momentum determines a positive sign of the Coulomb drag between clean one-dimensional (1D) quantum wires [1] and parallel 2DEGs in bilayer systems [2]. Interaction with the electromagnetic fluctuations is only possible for electrons confined in a quantum dot (QD) [3, 4, 5] thanks to a lack of momentum conservation. The speed of sound (v_s) being small makes it possible to absorb/emit acoustic phonons by both QD-confined [6] and freely moving 2DEG electrons [7]. In the last case, interaction with phonons of momenta as high as $2k_F$ and corresponding energies up to $2\hbar k_F v_s$ is allowed by conservation laws, where k_F and \hbar are, respectively, the Fermi momentum of the 2DEG, and the Planck's constant.

In this paper we overview a set of experiments on nonequilibrium interactions between neighboring electrically isolated nanostructures laterally defined within the 2DEG beneath the surface of a GaAs/AlGaAs heterostructure. The AFM micrograph of the sample is shown in Fig. 1a. The negatively biased central gate C depletes the underlying 2DEG and divides the sample into two coplanar nanostructures, defined and controlled by voltages on gates 1-10, with four separately contacted 2DEG leads (marked by crossed squares in fig. 1a). One of the nanostructures is an externally biased quantum point contact (drive-QPC) and is used to supply energy to the second nanostructure (detector). Absorption of energy results in generation of a dc current in the detector circuit, which is measured in the experiment. The energy spectrum of the excitation and its spatial asymmetry are studied by using a second QPC, a single QD or double quantum dot (DQD) as the detector. In all three cases the detection of quanta with energies up to ~ 1 meV occurs for bias voltages across the drive-QPC (V_{DRIVE}) in the mV range. The results suggest that the dominant energy transfer mechanism between the two quantum circuits in our experiment is based on

emission/absorption of nonequilibrium acoustic phonons happening in the 2DEG leads of the drive/detector nanostructure.

The paper is organized as follows. The details of the experiment are described in section II. The results for three detector realizations are presented in the subsequent sections III, IV and V. The discussion and following conclusions are given in the last section VI.

II. EXPERIMENTAL DETAILS

All the measurements presented below were performed on a GaAs/AlGaAs heterostructure, containing a 2DEG 90 nm below the surface, with a carrier density of $2.8 \times 10^{11} \text{ cm}^{-2}$ and a low-temperature mobility of $1.4 \times 10^6 \text{ cm}^2/\text{Vs}$. The metallic gate layout of fig. 1a was designed by means of e-beam lithography. The sample was immersed in the mixing chamber of a dilution refrigerator with a base temperature of 25 mK and cooled down to an electron temperature below 150 mK. Dc or low frequency (21 Hz) ac current measurements in the drive and detector circuits were performed by use of two current-voltage converters with variable gain from 10^6 to 10^9 V/A followed by a digital voltmeter or a lock-in amplifier, respectively. The lock-in technique was particularly useful for low-impedance counterflow measurements (see section IV), where the dc signal to noise ratio was poor. In some cases, a differential signal was obtained by numerically deriving the dc current data (section V) or vice versa (section IV). Measurements with interchanged signal and ground ohmic contacts, interchanged drive and detector nanostructures, as well as simultaneous dc and ac measurements, were performed to ensure the small signals measured are free from pick-up noise.

III. DOUBLE-DOT QUANTUM RATCHET

In this section we describe the experiment with a DQD in the detector circuit [8]. A sketch of the measurement is shown in fig. 1b. Two serially connected QDs with weak interdot coupling ($t \sim 0.1 \mu\text{eV}$) and strong dot-lead coupling ($\Gamma \approx 40 \mu\text{eV}$) are formed on one side of the gate C by negatively biased gates 1-5. Typical values of charging energy, single-particle level spacing and interdot Coulomb energy are, respectively 1.5 meV, $100 \mu\text{eV}$ and $100 - 200 \mu\text{eV}$. The charge configuration of the DQD is controlled by voltages V_2 , V_4

applied to gates 2 and 4, which predominantly couple to the electrochemical potentials of the right and left QD, respectively. A small bias voltage across the DQD $V_{\text{DQD}} = -20 \mu\text{V}$ is applied throughout the experiment.

In the absence of current in the drive-circuit ($V_{\text{DRIVE}} = 0$), I_{DQD} is mainly suppressed because of the Coulomb blockade (fig. 2a). The only exception is a pair of sharp resonances in the $[V_2, V_4]$ plain (so called stability diagram), where the electrochemical potentials of both dots μ_R , μ_L and 2DEG leads are aligned [9].

The situation changes drastically at finite bias across the drive-QPC, tuned halfway between the pinch-off and first conductance plateau ($g_{\text{DRIVE}} \equiv dI_{\text{DRIVE}}/dV_{\text{DRIVE}} \approx 0.5 G_0$, where $G_0 = 2e^2/h$ is the conductance quantum). In figure 2b I_{DQD} is plotted throughout the same region of the stability diagram for $V_{\text{DRIVE}} = -1.45 \text{ mV}$. In contrast to fig. 2a, now a nonzero current flows across the DQD in the regions of stable ground state charge configurations. The sign of the DQD current depends on the position in the stability diagram relative to the resonances. The current is negative on the left and above the resonances and positive on the right and below them ($I_{\text{DQD}} > 0$ corresponds to electrons moving to the left-hand side in the lower circuit of fig. 1b). I_{DQD} changes abruptly at the boundaries of stable ground state configurations, making them visible in fig. 2b (nearly horizontal and vertical lines originating from resonances, see Ref. [8] for details). Note that such a behavior is observed around many pairs of resonances in the stability diagram [10].

All the main features of fig. 2b can be explained by inelastic interdot tunnelling in the DQD, mediated by resonant absorption of an energy quantum from the drive-QPC circuit, similar to photon assisted tunnelling [9]. The energy absorbed by the top most DQD electron initially localized in one dot compensates for the difference of the dots' electrochemical potentials $\Delta \equiv \mu_L - \mu_R$ and lifts the Coulomb blockade of interdot and dot-lead tunnelling (see the insets of fig. 2c). This picture is further supported by the observed suppression of I_{DQD} inside a small diamond-shaped region between the resonances (fig. 2b). There, the excited state configuration is stable with respect to dot-lead tunnelling so that absorption of energy doesn't result in I_{DQD} [8].

Owing to the spatial asymmetry of the quantized charge distribution the DQD represents a realization of a quantum ratchet system [11] capable of rectifying nonequilibrium fluctuations in the environment. The resonant character of the rectification can be used for spectrometry of the excitation provided by the drive-QPC. In fig. 2c we plot I_{DQD} as a

function of Δ along the dashed trace in the stability diagram of fig. 2b for a set of V_{DRIVE} values (gate voltage to energy is converted with a standard calibration procedure [9]). At $|V_{\text{DRIVE}}| \gtrsim 1\text{mV}$ the ratchet contribution to I_{DQD} , which is odd in Δ , sets-in within about a 1 meV wide energy band $|\Delta| \lesssim 1\text{ meV}$.

Obviously, the energy transferred to the detector circuit is a part of the Joule heat dissipated in the drive circuit. However, the efficiency of this energization turns out to be a nonmonotonic function of the drive-QPC conductance. In figure 3a we show a color-scale plot of I_{DQD} as a function of V_{DRIVE} and gate voltage V_8 , which controls the drive-QPC conductance (fig 1b). Here, $\Delta = -450\text{ }\mu\text{eV}$. For comparison, a derivative of the drive-QPC conductance with respect to its gate voltage (below referred to as transconductance, $g_{\text{DRIVE}}^T = dg_{\text{DRIVE}}/dV_8$) is shown for identical axes in fig. 3b. In both figures, the dashed lines mark the boundaries between the so-called half-plateaus on the nonlinear differential conductance ($g_{\text{DRIVE}} \approx G_0/2$) and its pinch-off and first plateau ($g_{\text{DRIVE}} \approx G_0$). The plateaus and the boundaries between them appear as regions of low and high transconductance in fig. 3b [12]. As follows from figure 3a, at fixed V_{DRIVE} I_{DQD} is maximal on the drive-QPC half-plateau and suppressed on its first conductance plateau. In other words, the energization of the DQD ratchet is strong (weak) when the drive-QPC is tuned to a strongly nonlinear (almost linear) transport regime.

IV. COUNTERFLOW OF ELECTRONS IN ISOLATED QPCs

In the previous section we demonstrated that a broad-band energy transfer from the drive-QPC to the neighboring circuit can be detected with a quantum ratchet system. Here we analyze this energy flow placing a second QPC (detector-QPC) in the detector circuit, which represents a quantum system with no spatial asymmetry [13]. Both drive/detector QPCs have a one-dimensional (1D) subband spacing of about $4\text{ meV}/3\text{ meV}$, while the half-width of transition region between the quantized plateaus is $\delta \approx 0.5\text{ meV}$. Throughout this section we keep $g_{\text{DRIVE}} \approx 0.5 G_0$, which corresponds to the most pronounced effect. The sketch of the experiment is given in fig. 1c. The current generated in the unbiased detector circuit is measured as a function of V_{DRIVE} or gate voltage V_3 , which controls the position of the 1D subbands of the detector-QPC relative to the Fermi energy E_F of its 2DEG leads (thereby tuning its linear response conductance G_{DET}).

The detector current versus V_{DRIVE} is plotted in fig. 4 for two values of V_3 , which correspond to a position of the lowest 1D subband bottom E_0 well above E_F or almost aligned with it. At high enough $|V_{\text{DRIVE}}|$ a finite current is measured, which is positive/negative for $V_{\text{DRIVE}} < 0/ > 0$, i.e. it flows in the direction opposite to that of I_{DRIVE} . Below we refer to this current as a counterflow current I_{CF} . Note, that I_{CF} increases as E_0 approaches E_F from above, although much slower than the relative increment of G_{DET} . In figure 5a we compare the dependencies of G_{DET} and I_{CF} on V_3 in a wide range of gate voltages between the pinch-off and fully opened detector-QPC. The increase of G_{DET} is accompanied by strong oscillations of I_{CF} , which displays three well developed maxima before the detector-QPC is opened completely. The positions of maxima correspond to half-integer conductance values $G_{\text{DET}} \approx (i + 1/2)G_0$ attained each time the bottom of the i -th 1D subband $E_i \propto -|e|V_3$ ($i=0, 1, 2$) aligns with E_F .

Oscillations of I_{CF} are reminiscent of well-known oscillations of thermopower in single QPCs [14, 15]. In the absence of thermal equilibrium, the energy balance between the 2DEG leads of the detector-QPC is broken which results in net electric current:

$$I = \frac{2e}{h} \sum_i \int [f_R^l - f_L^r] T_i dE \quad (1)$$

Here, $f_R^l(E)$ ($f_L^r(E)$) is the average occupancy of the left (right) moving electron states in the right (left) 2DEG lead of the detector-QPC at energy E [16]. In thermopower experiments these are just Fermi-Dirac distributions with appropriate temperatures. The energy dependence of the i -th subband transmission probability evaluated in a saddle-point approximation [16] is given by $T_i = 1/(1 + \exp([E_i - E_F]/\delta))$, where δ is a half-width of the energy window corresponding to $0.25 < T_i < 0.75$. At temperatures low compared to δ thermoelectric current is proportional to $\sum dT_i/dE_i$, i.e. it oscillates as the QPC transconductance. The shape of the oscillations of I_{CF} in fig. 5a is indeed close to that of g_{DET}^T (solid line) [17]. This indicates that the counterflow effect is related to energetic imbalance between the two 2DEG leads of the detector-QPC. Note that a sign change of I_{CF} on the second quantized plateau could be ascribed to a slightly nonmonotonic behavior of G_{DET} in this region (i.e. $g_{\text{DET}}^T < 0$).

Despite this qualitative analogy, we find a remarkable quantitative disagreement between the thermoelectric model and experiment. In fig. 5b the counterflow data and g_{DET}^T are plotted on a logarithmic scale near the pinch-off ($E_0 \gg E_F$), where both decay nearly

exponentially with decreasing V_3 . In this regime, indeed, g_{DET}^T can be expressed as $g_{\text{DET}}^T \sim \exp(-[E_0 - E_F]/\delta)$. Importantly, I_{CF} decays much slower than g_{DET}^T , which is readily seen from the data for most negative V_3 . This means that electrons excited well above E_F are responsible for the counterflow in the pinch-off regime, i.e. $I_{\text{CF}} \sim \exp(-[E_0 - E_F - E^*]/\delta)$, where E^* is their characteristic excess energy. Standard gate voltage to energy calibration gives an estimate of $E^* \sim 0.5$ meV (see the scale bar in fig. 5b corresponding to $\Delta E_0 \approx 1$ meV). The thermoelectric model fails to simultaneously account for the energy scale E^* and measured I_{CF} values [18]. A leads temperature difference of about 3 K would be needed in the former case, which corresponds to thermal currents two orders of magnitude higher than actually measured (peak values ~ 10 nA versus ~ 100 pA in fig. 4). Hence, the above analysis shows that the distribution function of electrons in one of the detector leads is strongly non-thermal, out-weighted towards high excitation energies compared to the usual Fermi-Dirac distribution.

Finally, the observed direction of the counterflow defines the following empiric rule. The nonequilibrium lead of the detector-QPC is the one neighboring to the drain lead of the drive-QPC, i.e. the lead with the lower electrochemical potential where the electrons are being injected (see fig. 1c).

V. EXCITATION OF A QUANTUM DOT WITH AN ISOLATED QPC

In the last sections we showed how a generation of current occurs in the DQD- and QPC-based detector circuits neighboring the drive-QPC circuit. Here we demonstrate that a nonequilibrium excitation with a drive-QPC also influences the conductance of a single QD in the detector circuit. The sketch of the experiment is shown in fig. 1d. At fixed V_{DRIVE} the differential QD conductance g_{DOT} is measured in the linear regime as a function of gate voltage V_2 , which controls the dot's electrochemical potential. Throughout this section, again, $g_{\text{DRIVE}} \approx 0.5 G_0$.

In fig. 6 g_{DOT} is plotted versus V_2 for one relatively small and two much higher values of $|V_{\text{DRIVE}}|$. At small drive bias of 0.5 mV nonequilibrium excitation is ineffective (see two previous sections) and g_{DOT} shows three usual Coulomb blockade peaks. Two Coulomb valleys between the peaks are marked with numbers N and N+1 corresponding to the (unknown) total number of QD electrons in each case. Each of these peaks corresponds to an

equilibrium resonance condition, when the electrochemical potential of the QD aligns with that of the 2DEG leads (μ_{LEADS}). For instance, for the central peak this condition reads $E_{N+1}^g - E_N^g = \mu_{\text{LEADS}}$, where E_N^g denotes the total energy of the ground N-electron state of the QD. At high $|V_{\text{DRIVE}}|$ nonequilibrium excitation lifts the Coulomb blockade and g_{DOT} is strongly increased in Coulomb valleys (at least an order of magnitude). On top of a smooth background three resonant features are seen in Coulomb valleys in presence of excitation (see arrows). These correspond to the transport through the excited states of the QD.

In presence of excitation the QD is no longer at thermal equilibrium with its leads and its excited states are occupied with a probability much higher than that given by usual thermal fluctuations (exponentially small inside the Coulomb valley). In this case conductance peaks can be observed at different gate voltages, compared to the ground state resonances [5]. E.g. if E_N^* denotes the total energy of the excited N-electron state, an extra conductance peak corresponds to the resonance condition $E_N^* - E_{N-1}^g = \mu_{\text{LEADS}}$. This peak is shifted to a more positive gate voltage compared to the ground state Coulomb blockade peak: $\delta V_2 \propto (E_N^* - E_N^g)$. Similarly, the extra peak for $E_N^g - E_{N-1}^* = \mu_{\text{LEADS}}$ is shifted to a more negative gate voltage: $\delta V_2 \propto -(E_{N-1}^* - E_{N-1}^g)$. The resonances a/ b/ c in fig. 6 correspond to a set of such nonequilibrium transitions $\text{Ex}_N \leftrightarrow \text{Gr}_{N-1}$ / $\text{Ex}_{N+1} \leftrightarrow \text{Gr}_N$ / $\text{Ex}_{N+1} \leftrightarrow \text{Gr}_{N+2}$, where Ex (Gr) stands for excited (ground) many-electron states. The excitation energies deduced from the peaks positions equal $E_N^* \approx 530 \text{ } \mu\text{eV}$ and $E_{N+1}^* \approx 340 \text{ } \mu\text{eV}$ respectively for resonance a and resonances b, c.

Notably, only a few extra resonances are seen in fig. 6 despite the band-width of the drive-QPC excitation far exceeds a single-particle level spacing in our QD ($\sim 1 \text{ meV}$ versus $\sim 100 \text{ } \mu\text{eV}$). The reason why some resonances are most pronounced is probably related to optimal (maximal) ratio of the corresponding dot-lead tunnelling rate to the inelastic relaxation rate inside the dot. This idea can be directly verified by a measurement of the nonlinear differential conductance of the QD, where the excited states participate in transport thanks to a finite bias V_{DOT} across the QD. In fig. 7 we show a color-scale plot of g_{DOT} versus $[V_2, V_{\text{DOT}}]$ in the absence of nonequilibrium excitation. Diamond shaped regions of Coulomb blockade (Coulomb diamonds) are marked with corresponding electron numbers (same as in fig. 6). X-shaped regions of finite conductance, centered at the positions of zero bias Coulomb peaks, correspond to gate voltage range allowed for sequential tunnelling, which grows proportionally to $|V_{\text{DOT}}|$. At negative QD bias several lines of enhanced g_{DOT}

are distinguished below N+1-th and N-th Coulomb diamonds, which correspond to different excited states participating in transport at bias voltages $|V_{\text{DOT}}| > E^* - E^g$. The strongest among these resonances (marked with arrows) indeed correspond to the same excited states which are responsible for the extra resonances in fig. 6.

VI. DISCUSSION

In the above sections we demonstrated that the externally biased drive-QPC can provide a nonequilibrium excitation to the neighboring quantum circuit. The excitation has a large bandwidth of ~ 1 meV and can be detected with a QD, a DQD or a QPC placed in the detector circuit. Below we argue that the observation of the counterflow effect in the last case strongly favors an acoustic phonon based energy transfer mechanism.

The key ingredients necessary for the counterflow are (section IV): (i) absorption of energy quanta up to 1 meV by the free 2DEG electrons and (ii) preferential energy flow to one of the leads. The first requirement allows to rule out a possible contribution of electron-photon interaction based on conservation laws. Direct Coulomb interaction between the electrons of coplanar 2DEGs in the drive and detector circuits also cannot account for the counterflow. The momentum transferred via Coulomb interaction is restricted by the minimum distance between the electrons $|q| \leq 10^{-5} \text{ cm}^{-1}$ (gate C wider than 100 nm, see fig. 1a), which is much smaller than the Fermi momentum $k_F > 10^{-6} \text{ cm}^{-1}$. Under such conditions only a forward Coulomb scattering can occur, i.e. a mutual scattering of the two electrons moving in the same direction in different circuits, which obviously cannot give rise to the counterflow.

Both above conditions can be satisfied if electron-phonon interaction is taken into account. Thanks to its ballistic nature the current flowing across the drive-QPC results in injection of hot electrons above the Fermi energy into the drain lead, which leave unoccupied states (holes) below the Fermi energy in the source lead [19]. The drain electron and source hole excess energies (referred to respective Fermi energies $\epsilon_e^D = E - E_F^D > 0$ and $\epsilon_h^S = E - E_F^S < 0$) satisfy $\epsilon_e + |\epsilon_h| = |eV_{\text{DRIVE}}|$. Energy relaxation of nonequilibrium carriers in the drive-circuit can occur via emission of acoustic phonons. Part of the phonons with momenta parallel to the interface can be re-absorbed in the nearby detector circuit. Such phonons have momenta up to $2k_F$ and energies up to $2\hbar k_F v_s \approx 0.6$ meV (for sound velocity $v_s = 3 \cdot 10^5 \text{ cm/s}$) and can give rise to a strongly nonequilibrium distribution of electrons in the detector. Particularly

important for the counterflow effect is a nonlinear transport regime across the drive-QPC near its pinch-off [13]. Here the excess energies of the injected drain electrons are much higher than those of the source holes $\epsilon_h^S \ll \epsilon_e^D \approx |eV_{\text{DRIVE}}|$, so that the emission of phonons in the drive circuit occurs preferably at the drain side [20]. Because of the device geometry (fig. 1a), absorption of phonons in this case happens preferably in the neighboring lead of the detector circuit. This naturally explains the origin of the asymmetric excitation responsible for the counterflow and the sign of this effect.

Next we speculate how the acoustic-phonons-based energy transfer mechanism could explain our observations for the DQD quantum ratchet and QD excitation. In principle, high energy acoustic phonons can be directly absorbed by the localized QD electrons [6], which would suffice for a qualitative explanation. However, there exists an alternative microscopic mechanism. Strongly nonequilibrium electrons in the detector circuit create high frequency electric field fluctuations, which can in turn drive inelastic transitions in a QD and a DQD. In fact, the data of fig. 2c and fig. 6 look very similar to photon-assisted tunnelling data in DQD and QD under microwave excitation [9, 21]. We cannot unambiguously determine which of the two microscopic mechanisms is relevant for the excitation of the DQD ratchet and the QD in our experiments.

While in case of the counterflow a nonlinear transport regime in the drive circuit is responsible for the spatial asymmetry of the excitation, this condition is not necessary for the QD and DQD ratchet experiments. Still, we find that the excitation of both the DQD ratchet (see fig. 2) and the QD (not shown here) is suppressed at small drive bias $|V_{\text{DRIVE}}| \lesssim 1 \text{ mV}$ [22]. We attribute this drive-bias onset a rapid decrease of the electron-phonon energy relaxation rate at small excess energies in the so-called Bloch-Grüneisen limit. Indeed, in this limit a cooling power of the 2DEG can fall as $T_e^3 - T_l^3$ or faster at low temperatures in a polar crystal like GaAs [23] (T_e , T_l are the electron and lattice temperatures). In our case the situation is even more aggravated, because the emitted phonons have to be re-absorbed in the vicinity of the detector nanostructure. Therefore, the energy relaxation has to be spatially restricted to a length scale of about the 2DEG mean free path ($\approx 12 \mu\text{m}$). For comparison, the average path length an electron with $\sim 1 \text{ meV}$ excess energy travels before emitting an acoustic phonon can be considerably longer [23]. In the end, we would like to point out that the energy dependence of the electron-phonon relaxation rate alone fails to explain the enhanced efficiency of the DQD ratchet excitation

near the drive-QPC pinch-off (fig. 3a). Possibly some properties of the drive-QPC in the nonlinear transport regime and/or an alternative mechanism of the energy transfer could be relevant here, see e.g. [24].

In conclusion, we studied the energy transfer from an externally biased drive circuit containing a drive-QPC to a neighboring detector circuit containing a DQD, a QPC or a QD. In all three cases a 1 meV bandwidth excitation is observed. The main features of the experiments are explained within a qualitative model of acoustic phonon based energy transfer mechanism.

Acknowledgements

The authors are grateful to V.T. Dolgopolov, A.W. Holleitner, C. Strunk, F. Wilhelm, I. Favero, A.V. Khaetskii, N.M. Chtchelkatchev, A.A. Shashkin, D.V. Shovkun and P. Hänggi for valuable discussions and to D. Schröer and M. Kroner for technical help. We thank the DFG via SFB 631, the BMBF via DIP-H.2.1, the Nanosystems Initiative Munich (NIM) and VSK the A. von Humboldt foundation, RFBR, RSSF, RAS and the program "The State Support of Leading Scientific Schools" for support.

References

- [1] P. Debray et al., *J. Phys.: Condens. Matter* **13**, 3389, (2001); P. Debray et al., *Semicond. Sci. Technol.* **17**, R21, (2002)
- [2] T.J. Gramila et al., *Phys. Rev. Lett.* **66**, 1216 (1991)
- [3] R. Aguado, L.P. Kouwenhoven *Phys. Rev. Lett.* **84**, 1986 (2000)
- [4] S. Gustavsson, M. Studer, R. Leturcq, T. Ihn, K. Ensslin, D.C. Driscoll, A.C. Gossard *Phys. Rev. Lett.* **99**, 206804 (2007)
- [5] E. Onac, F. Balestro, L.H. Willems van Beveren, U. Hartmann, Y.V. Nazarov, L.P. Kouwenhoven *Phys. Rev. Lett.* **96**, 176601 (2006)
- [6] L. Fedichkin, M. Yanchenko, K.A. Valiev *Nanotechnology* **11** 387 (2000)

- [7] V. F. Gantmakher and Y. B. Levinson, in *Carrier Scattering in Metals and Semiconductors* (North-Holland, Amsterdam, 1987)
- [8] V.S. Khrapai, S. Ludwig, J.P. Kotthaus, H.P. Tranitz, W. Wegscheider Phys. Rev. Lett. **97**, 176803 (2006)
- [9] W.G. van der Wiel et al., Rev. Mod. Phys. **75**, 1 (2003)
- [10] V.S. Khrapai, S. Ludwig, J.P. Kotthaus, H.P. Tranitz, W. Wegscheider Phys. E **40**, 995 (2008)
- [11] P. Reimann Phys. Rep. **361**, 57 (2002); P. Reimann, P. Hänggi, APL A **75**, 169 (2002); S. Kohler, J. Lehmann, P. Hänggi Phys. Rep. **406**, 379 (2005)
- [12] A. Kristensen et al., Phys. Rev. B **62**, 10950 (2000)
- [13] V.S. Khrapai, S. Ludwig, J.P. Kotthaus, H.P. Tranitz, W. Wegscheider Phys. Rev. Lett. **99**, 096803 (2007)
- [14] L.W. Molenkamp et al., Phys. Rev. Lett. **68**, 3765 (1992); H. van Houten et al., Semicond. Sci. Technol. **7**, B215 (1992)
- [15] A.S. Dzurak et al., J. Phys.: Condens. Matter **5**, 8055, (1993)
- [16] see M. Büttiker Phys. Rev. B **41**, 7906 (1990) and references therein.
- [17] A poor comparison between I_{CF} and g_{DET}^T for the left-most peak in fig. 5a is related to the so-called 0.7 anomaly in detector conductance, which causes the asymmetry of the g_{DET}^T peak. This effect is usually attributed to interactions, hence the single-particle approximation to thermopower is not likely to be accurate in this region.
- [18] We note that the saddle-point model [16] used is not fully consistent with the experimental dependence of G_{DET} on V_3 . E.g. a proportionality $g_{DET}^T \propto T_0 \cdot (1 - T_0)$ predicted by the model is not exactly fulfilled in our experiment (compare solid and dashed lines in fig. 5b). Such minor discrepancies do not effect our conclusions about the relation between thermopower and counterflow.
- [19] Here we choose the source/drain to be the lead with the higher/lower electrochemical potential, so that $\mu_{\text{DRIVE}}^S = \mu_{\text{DRIVE}}^D + |eV_{\text{DRIVE}}|$ (note the definition dependence on the sign of V_{DRIVE}).
- [20] A. Palevski et al., Phys. Rev. Lett. **62**, 1776 (1989)
- [21] T.H. Oosterkamp, L.P. Kouwenhoven, A.E.A. Koolen, N.C. van der Vaart, C.J.P.M. Harmans Phys. Rev. Lett. **78**, 1536 (1997)
- [22] Note, that suppression of the excitation at low bias doesn't allow us to observe a minimum bias condition for single-quanta excitation at certain energy $|V_{\text{DRIVE}}^{\min}| \geq |E/e|$, which was

verified in shot-noise detection [4, 5].

[23] B.K. Ridley, Rep. Prog. Phys **54**, 169 (1991)

[24] A.L. Chudnovskiy, arXiv:0710.2403v1

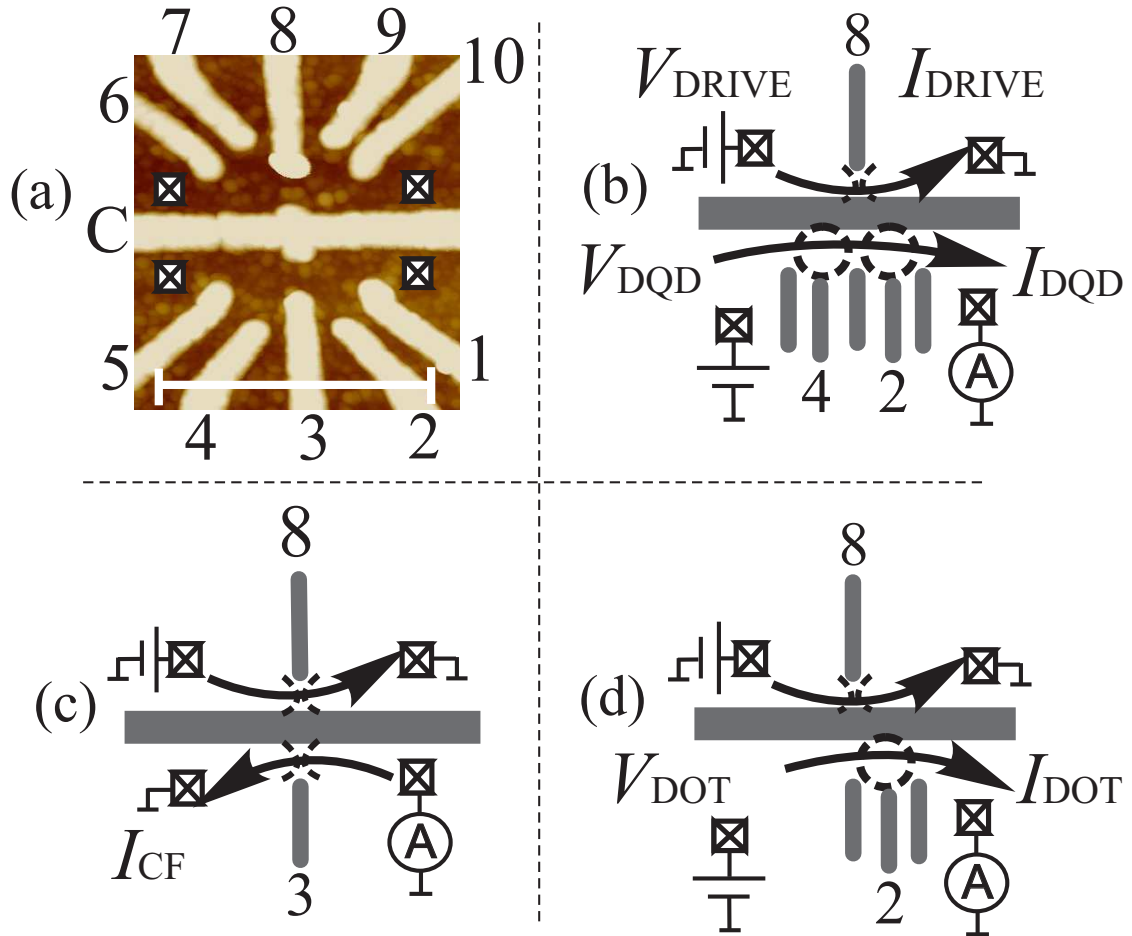


FIG. 1: (a): AFM micrograph of the nanostructure. Metal gates on the surface of the heterostructure are shown in bright tone. Crossed squares mark contacted 2DEG regions. The scale bar equals $1 \mu\text{m}$. (b),(c),(d): sketches of the measurement configuration for three different realizations of the detector nanostructure. Gates used in each case are shown in dark.

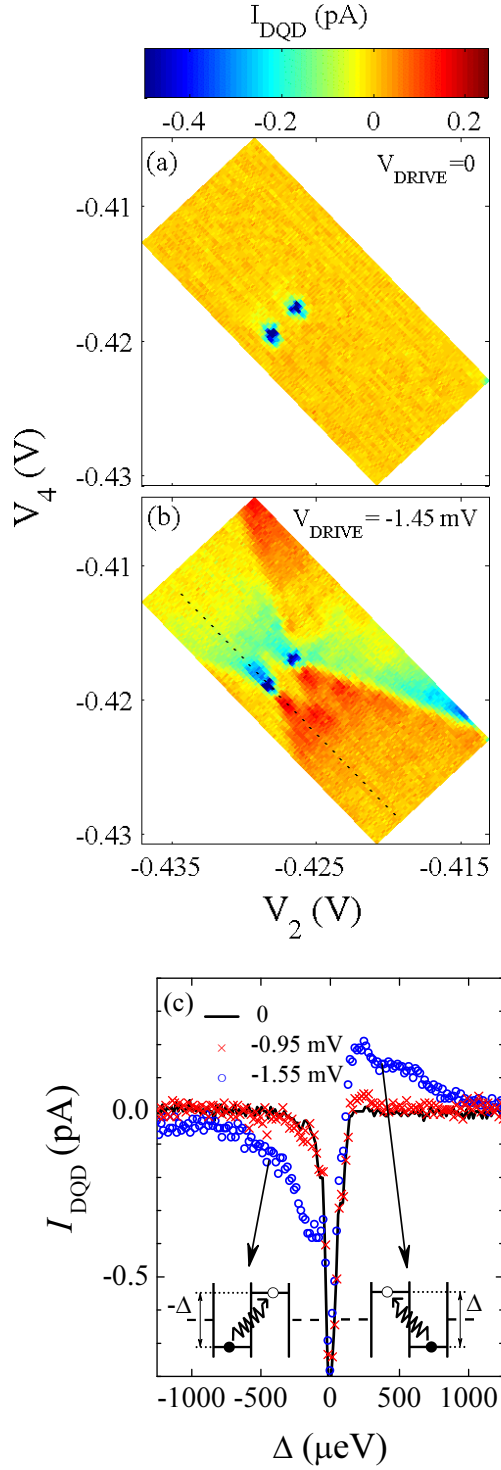


FIG. 2: (a),(b): Color-scale plot of I_{DQD} for two corresponding values of V_{DRIVE} . The top color-bar is the same for both panels. (c): I_{DQD} vs the electrochemical potential difference between the two dots, taken along the dashed trace in (b) for three values of V_{DRIVE} . The left/right inset schematically shows the inelastic interdot tunnelling processes responsible for negative/positive ratchet contribution to I_{DQD} .

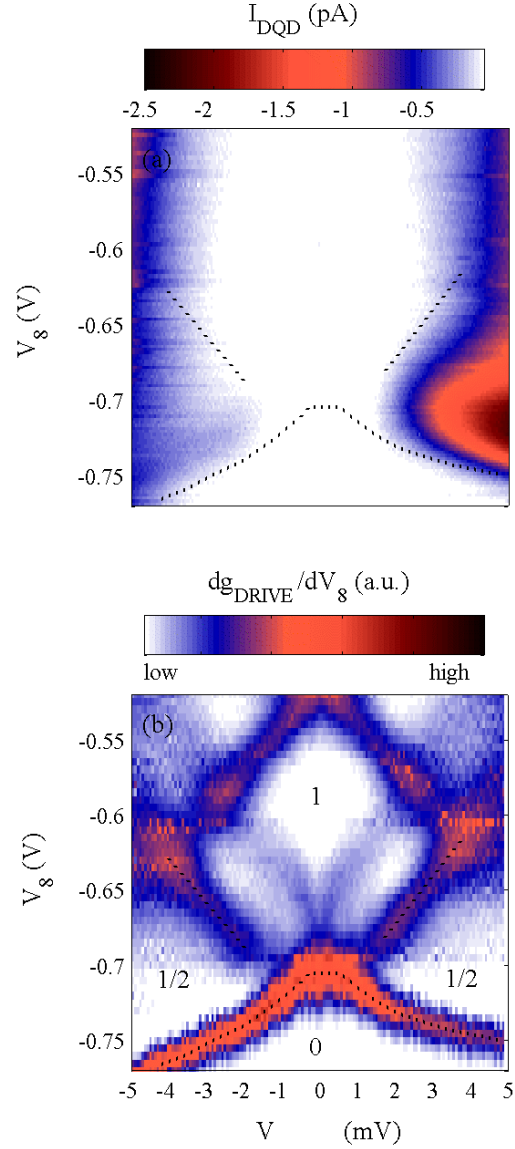


FIG. 3: (a): Color plot of I_{DQD} vs bias and gate voltage of the drive-QPC. (b) Color plot of g_{DRIVE}^T for the same region of the $[V_{\text{DRIVE}}, V_8]$ plain. Low g_{DRIVE}^T regions are marked by corresponding approximate values of g_{DRIVE}/G_0 . In both figures dashed guide-lines mark the boundaries of half integer plateaus on g_{DRIVE} .

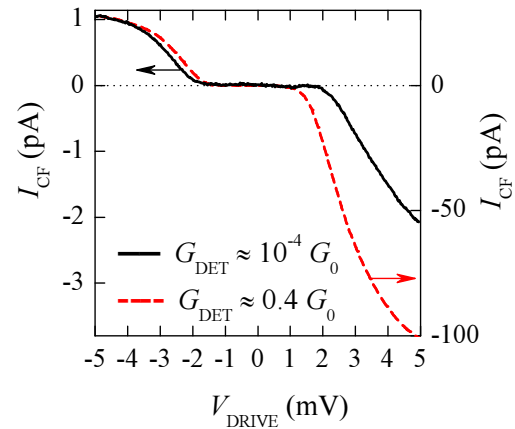


FIG. 4: Current through the detector-QPC as a function of bias across the drive-QPC. The data for two indicated values of the detector-QPC conductance are plotted on corresponding left and right ordinate scales.

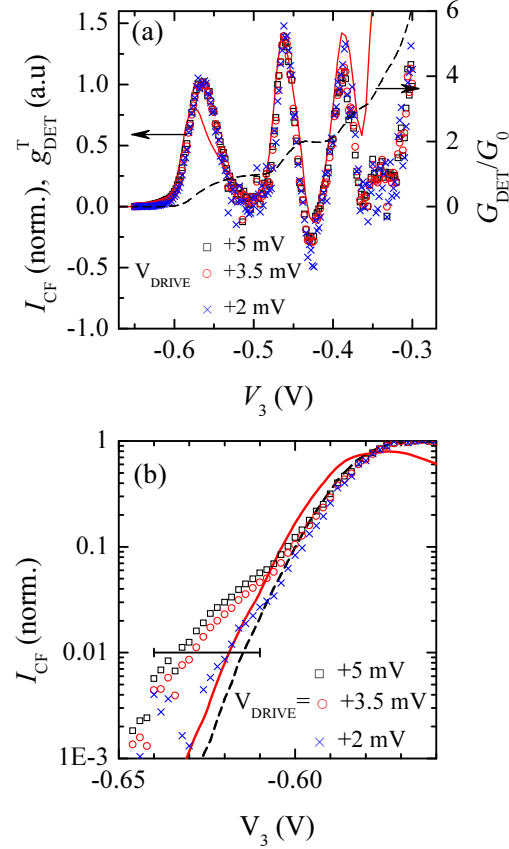


FIG. 5: (a): I_{CF} vs V_3 normalized by its leftmost peak value for a set of V_{DRIVE} values (left panel). Conductance (dash) and transconductance (solid line) of the detector-QPC (right panel). (b): Log-scale of I_{CF} near detector pinch-off. g_{DET}^T (same units as in (a)) and transmission function $T_0(1 - T_0)$ of the detector-QPC are also shown as solid and dashed lines respectively. The bar indicates a gate voltage scale corresponding to a change of $E_0 - E_F$ by 1 meV.

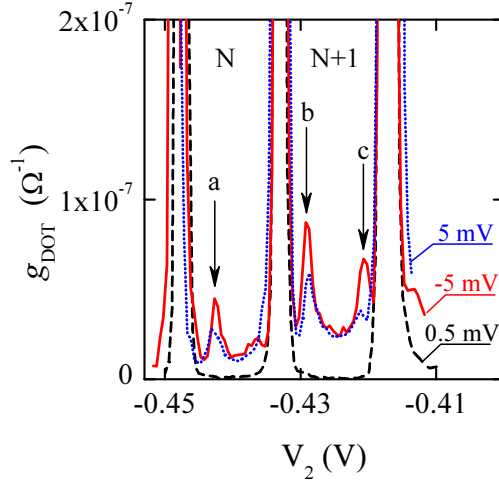


FIG. 6: Differential conductance of the QD in the detector circuit vs gate voltage for three values of V_{DRIVE} . Three peaks in the Coulomb valleys (arrows a,b,c) correspond to conductance through excited QD states.

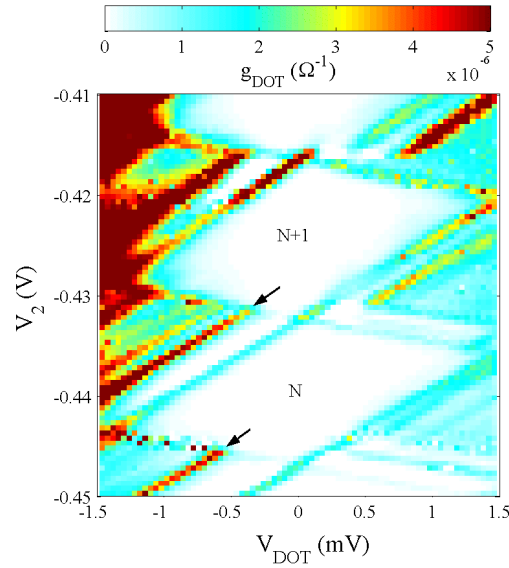


FIG. 7: Color-scale plot of the QD's differential conductance in the absence of nonequilibrium excitation with the drive-QPC ($V_{\text{DRIVE}} = 0.5$ mV). Arrows indicate the two strongest source-resonances corresponding to transport through $N+1$ -electron and N -electron excited QD states.